Supplemental Material

Table S7. Number of floods and intermediate calculations.

Table S8. Sensitivity of bin width and smoothing distance.

Lehnigk, K. E., Larsen, I. J., Lamb, M. P., David, S. R. 2024. Rates of bedrock canyon incision by megafloods, Channeled Scabland, USA: Geological Society of America Bulletin, https://doi.org/10.7275/8zws-f751.

SUPPLEMENTAL TEXT S1

Introduction

The Supplementary Text outlines sensitivity testing efforts in Douglas Creek and provides additional details on the topographic reconstruction of upper Grand Coulee, Moses Coulee, and Wilson Creek. Supplementary Figures include maps referenced in the main text regarding regional geology, topographic reconstruction results, hydraulic modeling domains, hydraulic modeling inundation results, and hydraulic modeling shear stress results, as well as maps and figures regarding the sensitivity analysis at Douglas Creek. Supplementary Tables include detailed data referenced in the main text including lists of tributaries classified as outliers during the topographic reconstruction process, well log data, results from additional hydraulic models not discussed in the main text, terrestrial flood deposits, sensitivity of flood number estimates to suspended-to-bedload sediment ratio, and intermediate values from the calculation of the number of floods, as well as detailed data related to sensitivity testing.

Sensitivity Analysis at Douglas Creek

Introduction

Douglas Creek (Figure S12), a tributary of Moses Coulee which was not significantly modified by floods (Bretz et al., 1956), was used to determine the parameters which would yield the most accurate reconstruction for flood-carved canyons in the Channeled Scablands. We generated a uniform 1,000 m buffer distance on either side of Douglas Creek to produce an

artificial "canyon" with a 2,000 m width comparable to mean widths of upper Grand Coulee, Moses Coulee, and Wilson Creek. The topography within the buffer was masked, and the tributaries which drain to Douglas Creek were used to reconstruct its profile and topography using the same approach described for the three flood channels examined in the main text. The elevations of the reconstructed trunk stream profile and interpolated topography within the buffered reach were then compared with the actual elevations, and the hydraulics of flows on both the original and reconstructed surfaces were compared.

Methods

Topographic reconstruction Comparisons of elevations from extrapolated tributaries, smoothed long profiles, and interpolated 2D surfaces with the actual topography allowed us to assess the accuracy of the reconstruction method. We tested three methods for determining the orientation of the extrapolated stream reaches using the tributaries of Douglas Creek: 1) the average orientation of the channel 500 m upstream of the artificial canyon "rim", 2) the average orientation between the artificial canyon "rim" and the next confluence with another tributary upstream, and 3) the orientation between the artificial canyon "rim" and the point on the Douglas Creek trunk stream located closest to the artificial canyon "rim". We explored several methods of interpolating surfaces between the canyon rims and the reconstructed long profile in ArcMap; these included: Triangular Irregular Network (TIN), Natural Neighbor, Spline, Trend, and Topo To Raster. We also generated a smoothed version of the present-day DEM, in which topography within the extent of the reconstructed area was smoothed using a focal statistics smoothing algorithm with a square 50-cell moving window, to evaluate the effects of the loss of topographic complexity inherent in the 2D surface interpolation process.

Discharge reconstruction To compare the inundation extents and shear stresses produced by flows over the present-day topography to those for flows over the reconstructed topography, we modeled discharges of 1,000, 2,000, and 3,000 m^3s^{-1} on each surface. A constant discharge was introduced across the inlet boundary at the upstream end of Douglas Creek for 250,000 s, until steady-state conditions were achieved (Lehnigk and Larsen, 2022). All boundary segments were modeled as Dirichlet boundaries to allow flows to exit the domain, except for the inlet, which was modeled as a reflective boundary (Figure S13). A spatially uniform Manning roughness coefficient of 0.065 was used, representative of roughness values in Moses Coulee (Larsen and Lamb, 2016), and the maximum triangle area of the computational mesh was 5,000 m^2.

Results

Topographic reconstruction The three methods for determining the orientation of extrapolated stream reaches produced similar error between the extrapolated outlet elevation and the actual elevation of the profile at that point, with an average elevation offset of 19.2 m using the azimuth from 500 m upstream from the artificial canyon "rim," 20.2 m using the azimuth from the first confluence to the artificial canyon "rim," and 18.5 m using the azimuth from the artificial canyon "rim" to the closest point on Douglas Creek. However, the reconstructed long profile using the closest point method had a root-mean-square error of 23.0 m between the full interpolated profile and the full true profile, while the 500 m method had a root-mean-square error of 18.3 m and the first confluence method had a root-mean-square error of 19.2 m. Therefore, the orientation along which each hanging tributary's profile was extended was determined by the average azimuth of

the tributary over the shorter of either 500 m upstream of the rim or the distance from the rim to the first confluence upstream.

The difference in elevation between the reconstructed profiles and the actual profiles of tributaries of Douglas Creek appeared to be correlated with the length of the tributary, the number of binned points used to calculate k and λ, extreme values for λ, and the length of the extrapolated reach (indicating a highly oblique intersection of the projected stream with the trunk stream). The mean elevation offset between the extrapolated outlet elevation and the true elevation at the junction with the trunk stream was reduced from 19.2 m (n = 73) to 17.2 m (n = 42) for profile extrapolations using the first 500 m upstream of the artificial canyon rim, and from 20.2 m (n = 74) to 18.1 m (n = 41) for profile extrapolations using the distance to the first confluence, after eliminating tributaries with 3 or fewer binned points comprising the upstream reach (labeled "short fit" in Tables DR1 – DR3), a concavity index λ less than -2 or greater than -0.1, an extrapolation length greater than 1.5 times the width of the artificial canyon mask, or a fitted reach that was less than half of the width of the artificial canyon mask.

Testing our long-profile reconstruction method on Douglas Creek shows that the predicted long profile reasonably approximates the actual long profile (Figure S14). The root-mean-square error between the reconstructed profile and the actual profile using the "rloess" smoothing algorithm (Savitzky and Golay, 1964) is 16.7 m, which is 2.8% of the total profile relief. Most of the error is due to misfit in the downstream-most channel reach, which is potentially due to headward knickzone migration as the channel has eroded into a sedimentary interbed between basalt flows. Hence, the fit in the lower reach of Douglas Creek may not be representative of areas where the channel was incised into basalt. We also tested the "loess" smoothing method, an unweighted linear least squares 2nd-order polynomial model, to generate

the long profile (Savitzky and Golay, 1964), which produced a slightly higher but still minimal root-mean-square error of 18.1 m (3.1% of the total relief).

The Topo to Raster interpolation method was selected to generate the pre-incision surface because this tool enforces connectivity of geomorphic features such as streams, valleys, and ridges (Hutchinson et al., 2011), and because it reproduced the true valley topography well, with a mean elevation error of -7.3 m and 95% of elevations differing by <10 m (Figure S15). Such elevation differences are a small fraction of the depth of Moses Coulee and Grand Coulee, but comparable to the mean incision depth for Wilson Creek of 10 m.

Discharge reconstruction Shear stresses and high-water predictions for floods routed across the reconstructed and present-day Douglas Creek topography are similar, with medians of 85 Pa and 103 Pa and interquartile ranges of 40 – 156 Pa and 35 – 177 Pa generated by a discharge of 2,000 m^3s^{-1} run for 250,000 s to steady state on the present-day and reconstructed topography, respectively. Based on the absolute value of the difference raster computed between modeled stages on the present-day and reconstructed topography, we found that 69% of stages modeled over the two topographies are within 5 m of each other. The wetted extent on the smoothed topography after 250,000 s of 2,000 m^3s^{-1} flow is similar to the wetted extent for the equivalent flow over the present-day topography (Figure S13), and 87% of stages are within 5 m of each other, suggesting that the loss of topographic complexity inherent in our reconstruction method is negligible for the purpose of estimating flood size and erosion capacity. Hence, we infer that our method of topographic reconstruction generates reasonable predictions of flood hydraulics.

Additional details regarding topographic reconstruction of upper Grand Coulee, Moses Coulee, and Wilson Creek

Elevation profiles were extracted for all tributaries, identified by the D8 flow algorithm, which had a clearly defined slope break at the intersection with the canyon and had a projected azimuth that intersect the canyon midline, resulting in a total of 211 tributaries. Tributaries which had qualities that lowered the accuracy of the Douglas Creek reconstruction—namely 3 or fewer binned points comprising the upstream reach, a concavity index λ less than -2 or greater than -0.1, an extrapolation length greater than 1.5 times the width of the canyon, or a fitted reach that was less than half of the width of the canyon—were removed from the population used to reconstruct the pre-incision valley profile for each canyon. Tributaries whose entire lengths were located within surficial geologic units mapped as glacial- and flood-eroded (Figure S1; Washington Division of Geology and Earth Resources, 2010) were also removed, as erosion by floods or glaciers, indicated by characteristics such as removal of loess, likely altered the topography such that the tributary elevation profiles would not reflect steady-state conditions. In total, 73 tributaries were removed from the total 211 tributaries for which elevation profiles were extracted. A summary of removed tributary characteristics is included as Tables S1 – S3, and a complete list of tributary characteristics for upper Grand Coulee, Moses Coulee, Wilson Creek, and the test stream Douglas Creek, including removed tributaries, is included in the Data Repository ("all_trib_notes_KL.xls").

Sensitivity analysis of bin width and smoothing window width of tributaries was performed on 10 of the tributaries draining into Grand Coulee and Moses Coulee by comparing the extrapolated elevation 500 m from the rim for the different bin widths and the elevation of the selected rim point for the different smoothing window widths (Table S8). Fixed bin widths of

25, 50, 100, and 200m were assessed, as well as a distance that grew logarithmically with distance downstream by dividing the tributary length into $10\log(distance_{max} - 1)$ bins each with a width of $10^{bin\ number}$. Five smoothing options, with units of points extracted from the 10 m DEM, were assessed: 5, 10, 25, 50, and no smoothing. Extrapolated elevations were found to vary <10 m for bin widths of 25, 50, and 100 m; 100 m was therefore selected as the bin distance to ensure at least 5 points per bin. Rim elevations were found to vary <1 m for smoothing windows of 0, 5, 10, 25, and 50 m; 50 m was therefore selected as the smoothing window width to make it easier to distinguish the rim.

The present-day topography includes sediment deposited in the three valleys postdating incision. The additional elevation from sedimentary deposits is likely minimal in upper Grand Coulee, but may constitute a larger fraction of the removed volume in Moses Coulee and Wilson Creek (Hanson, 1970). To evaluate the sediment thickness in the three canyons, we aggregated well log data within each canyon from the Washington Department of Ecology's online well log database (https://appswr.ecology.wa.gov/WellConstruction/Wells/PublicPages/WellConstructionAndLicensingHome.aspx), and determined the sediment depth for all wells within 250 m of the midline or cross sections for each canyon (Figure S2). Of the wells that included information on the sedimentary units, sediment depths from wells which were entirely located within unconsolidated sediments were characterized as minimum sediment depths, whereas sediment depths from wells which include bedrock or 'angular basalt' in lower units were characterized as approximate sediment thicknesses. Sediment deposit thickness ranges from 0 – 33 m in upper Grand Coulee, 0 – 77 m in Moses Coulee, and 0 – 41 m in Wilson Creek. Several of the predicted tributary junction elevations in Moses Coulee and Wilson Creek projected below the

present-day topographic surface, and our reconstructed long profiles predict the pre-flood

bedrock surface to be slightly below the present-day topographic surface in the downstream

reach of Moses Coulee and the upstream reach of Wilson Creek (Figure 3), suggesting that the

hanging tributary reconstruction method produces a reasonable estimate of pre-flood topography.

However, due the additional elevation contributed to the present-day topography by sedimentary

deposits, our estimates of eroded bedrock volume should be considered minimums.

SUPPLEMENTARY FIGURES
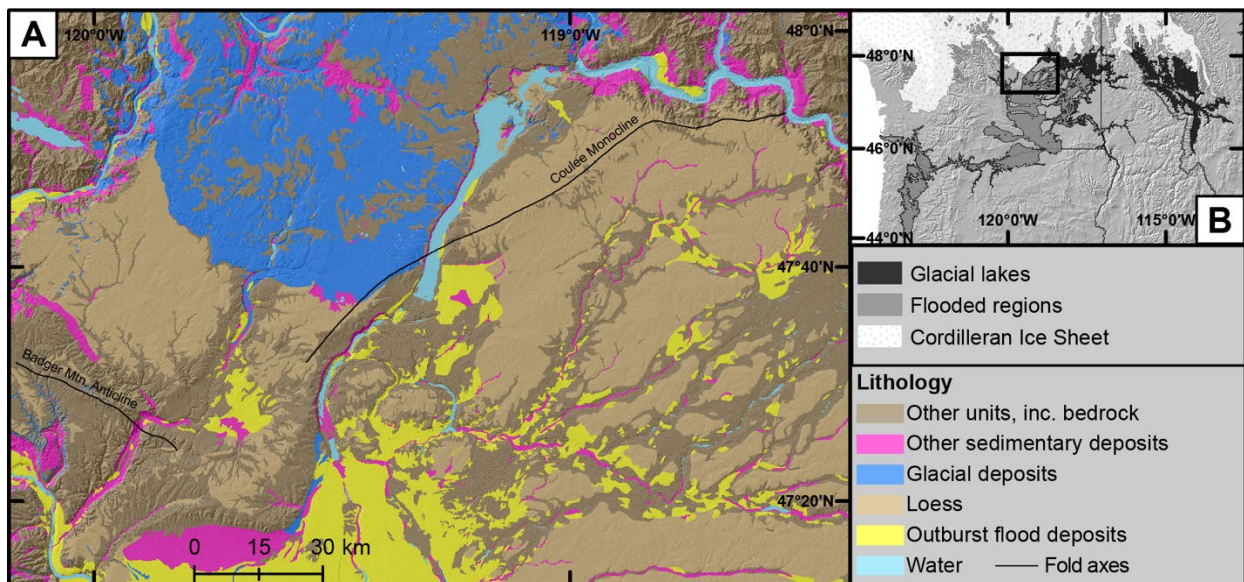
Figure S1. A) Simplified map of geologic units from the Washington Division of Geology and

Earth Resources (2010) mapped at a scale of 1:100,000, used to classify drainage basins in the

topographic reconstruction step as flood- or glacier-modified and remove them from the

population used to reconstruct pre-incision long profiles. B) The location of the study area in the

northwestern USA showing the locations of ice lobes, glacial lakes, and areas inundated by

Missoula floods during the last glaciation (Ehlers et al., 2011).
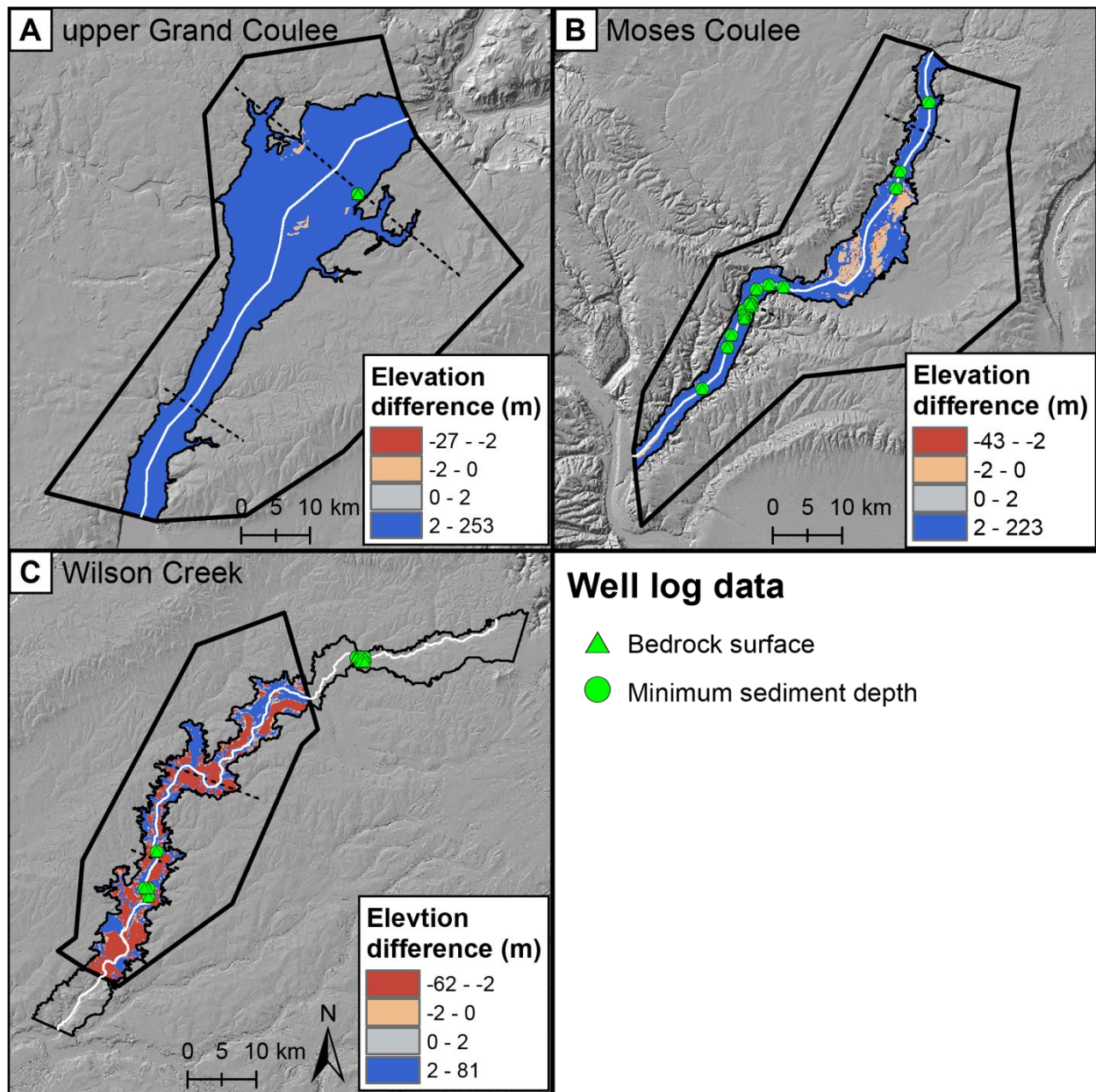
Figure S2. Elevation difference between reconstructed and present-day topography for upper Grand Coulee (A), Moses Coulee (B), and Wilson Creek (C). The thin black outline indicates the extent of reconstruction, while the thick black polygon indicates the extent of the hydraulic modeling domain for each canyon. Well locations within 250 m of either the canyon midline (white line) or the cross sections in Figure 4 (dashed black lines) are indicated as green triangles

for wells that indicated a depth to bedrock, and green circles for wells entirely in unconsolidated sediments.
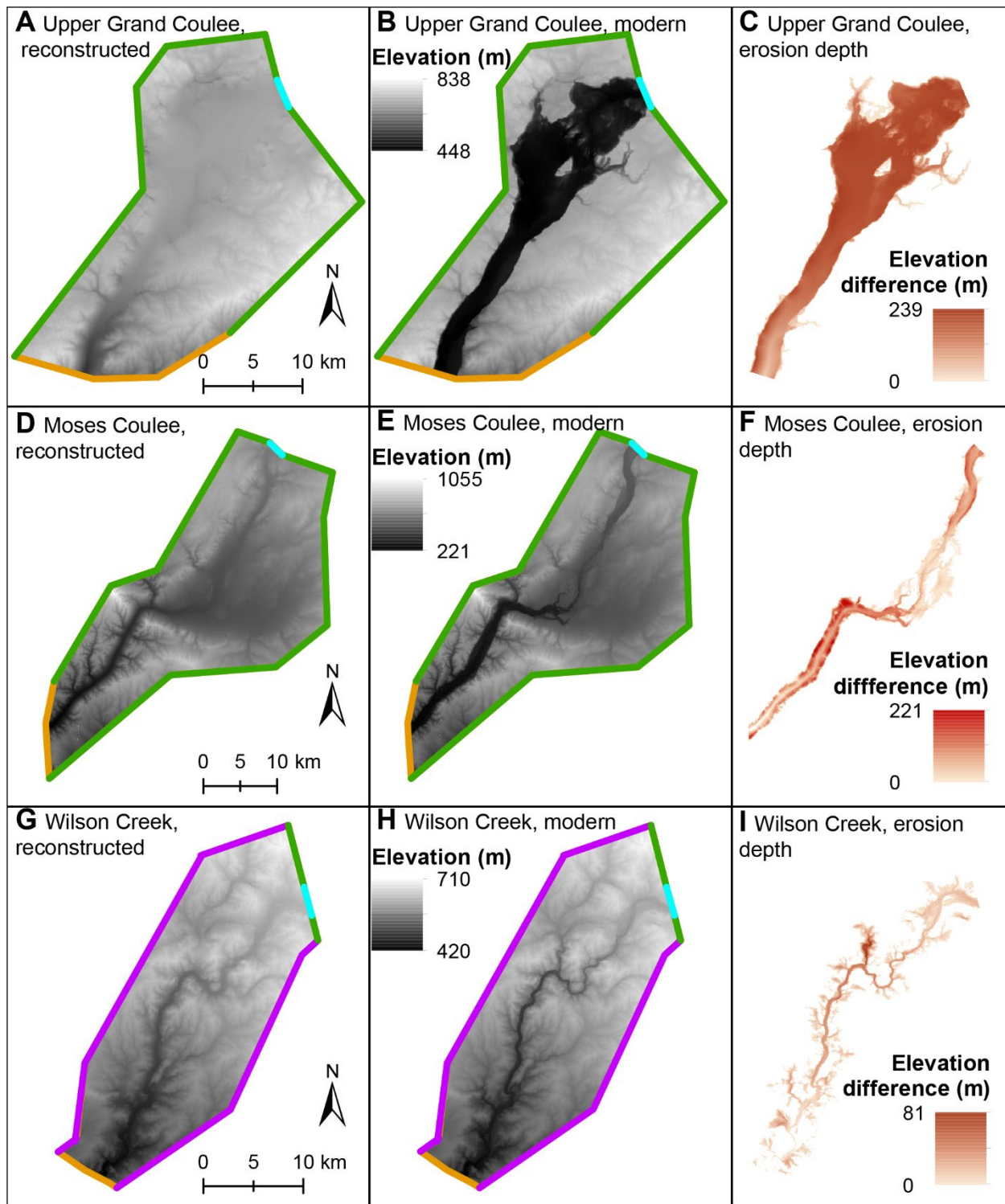
Figure S3. Domains and boundary conditions for hydraulic models on upper Grand Coulee (A, B, & C), Moses Coulee (D, E, & F), and Wilson Creek (G, H, & I), using the reconstructed topography (A, D, & G) and the present-day (modern) topography (B, E, & H), with the

difference in elevation between the two shown in C, F, & I. Orange lines indicate open

boundaries, green lines indicate closed boundaries, purple lines denote a boundary that was

either open or closed depending on the model run, and the light blue line indicates the discharge

inlet.
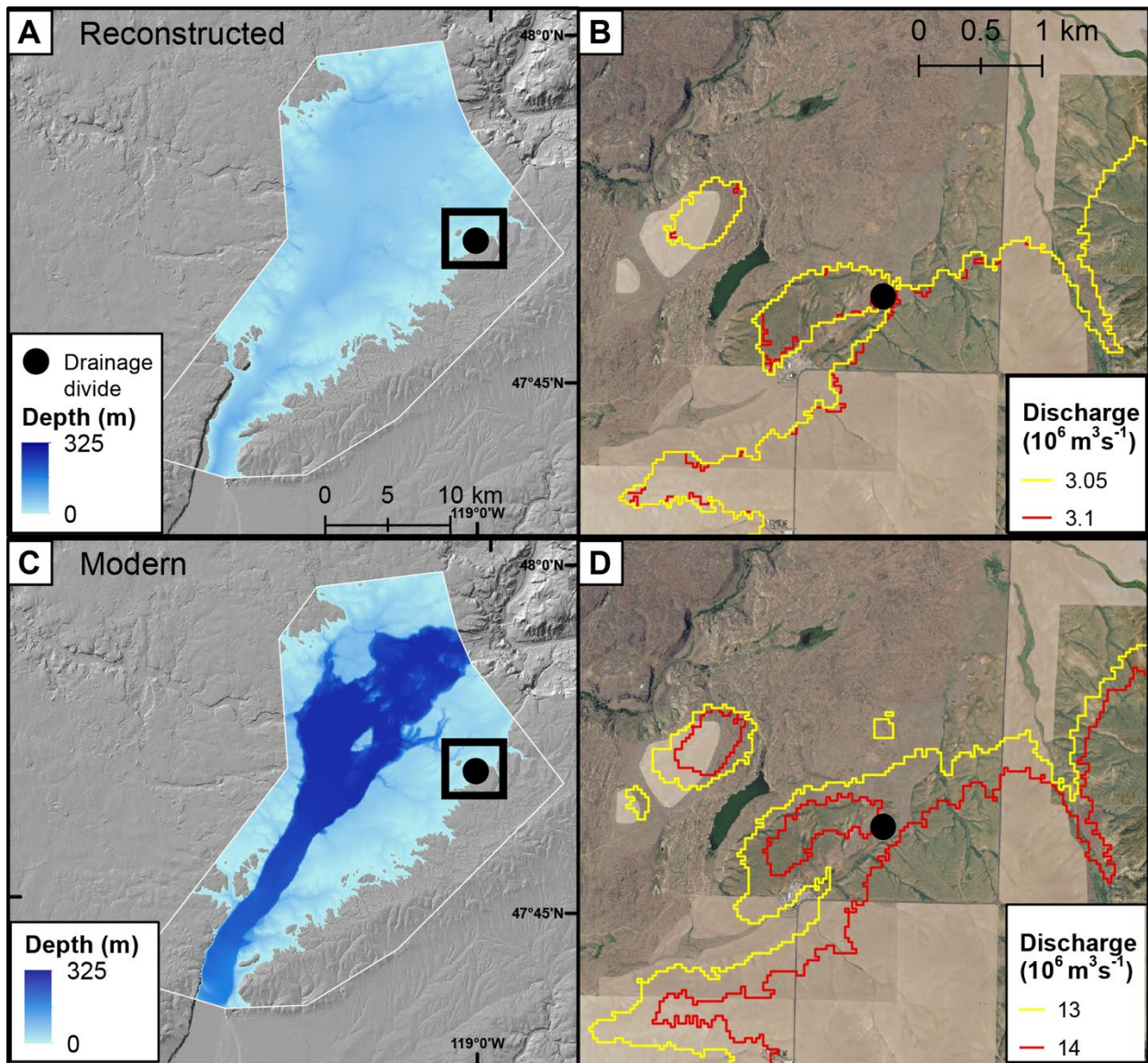
Figure S4. The high-water-inundating discharge for upper Grand Coulee. (A) Depth of the 3.1×10^6 m^3 s^{-1} discharge, which is the minimum flow required to inundate the high-water mark on reconstructed pre-flood topography. (B) The shallow drainage divide on the east rim (black circle) is crossed at a discharge of 3.1×10^6 m^3 s^{-1} on reconstructed topography. (C) Depth of the 14×10^6 m^3 s^{-1} discharge, which is the minimum flow required to inundate the high-water mark on present-day (modern) topography. (D) The shallow drainage divide on the east rim (black circle) is crossed at a discharge of 14×10^6 m^3 s^{-1} on present-day topography.
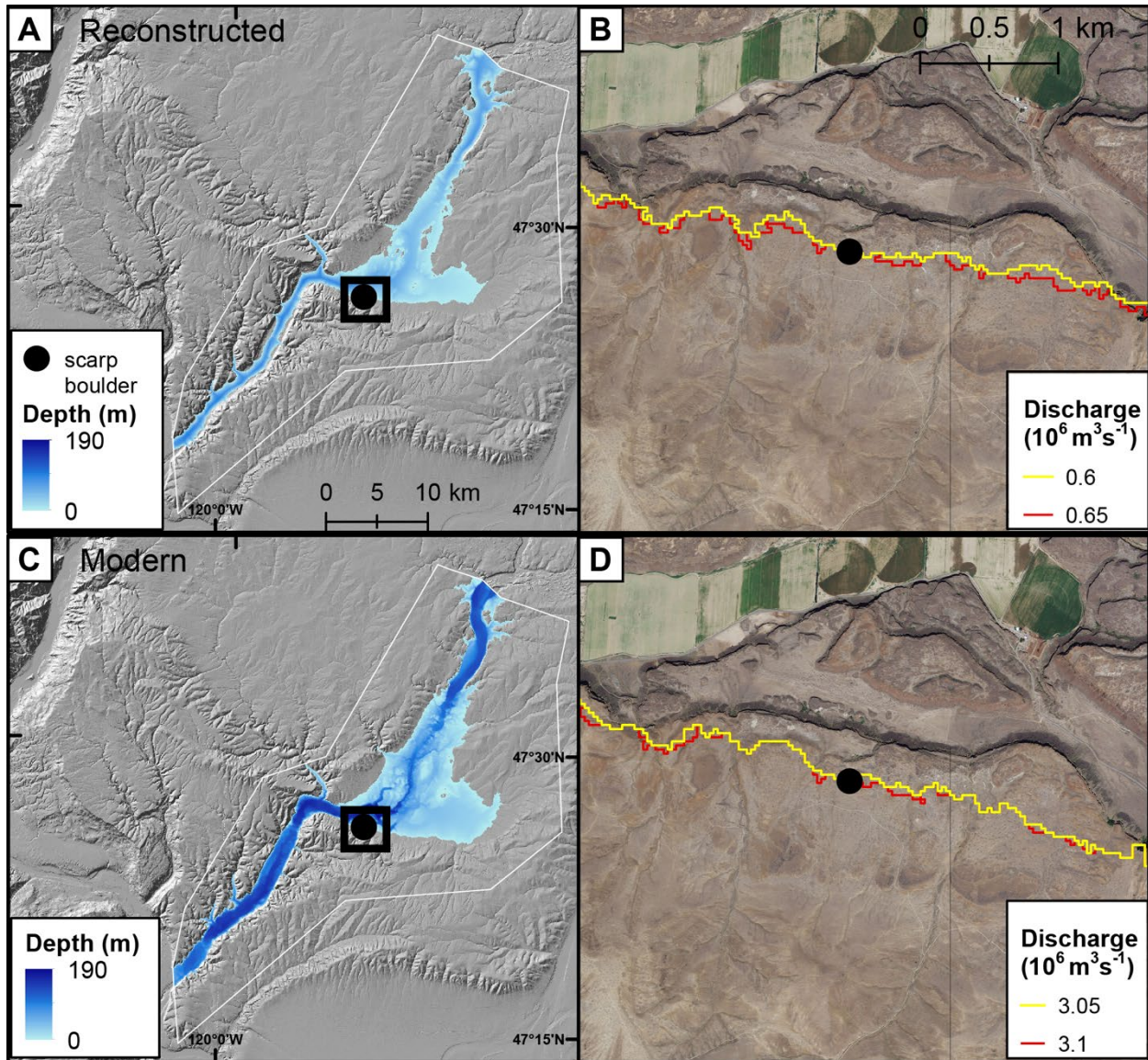
Figure S5. The high-water-inundating discharge for the scarp boulder at Moses Coulee. (A) Depth of the 0.65×10^6 m^3 s^{-1} discharge, which is the minimum flow required to inundate the high-water mark on reconstructed pre-flood topography. (B) The flood-transported boulder along the eroded loess scarp (black circle) is crossed at a discharge of 0.65×10^6 m^3 s^{-1} on reconstructed topography. (C) Depth of the 3.1×10^6 m^3 s^{-1} discharge, which is the minimum flow required to inundate the high-water mark on present-day (modern) topography. (D) The

flood-transported boulder along the eroded loess scarp (black circle) is crossed at a discharge of 3.1×10^6 m³ s⁻¹ on present-day topography.
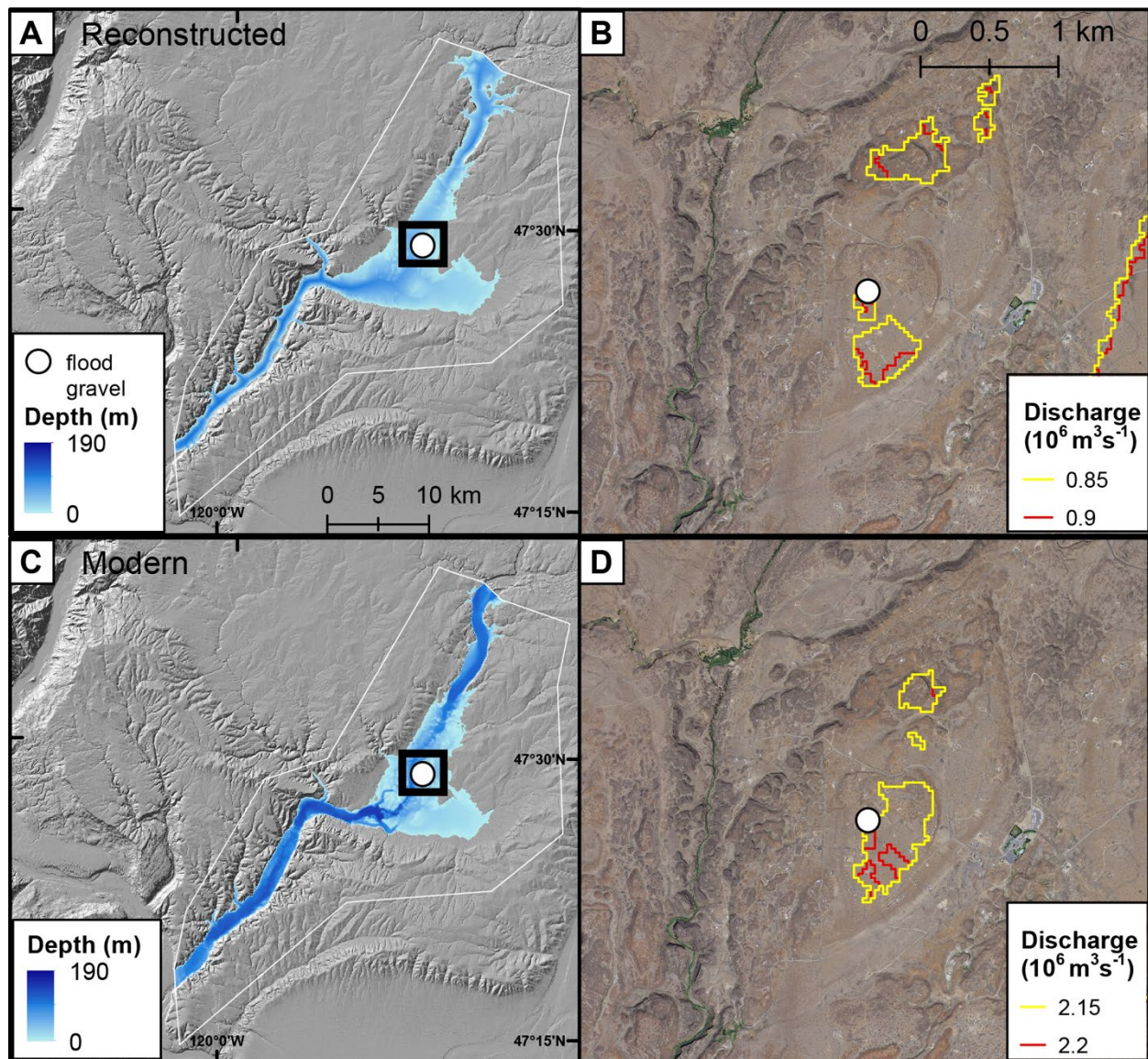
Figure S6. The high-water-inundating discharge for the flood gravel at Moses Coulee. (A) Depth of the 0.9×10^6 m³ s⁻¹ discharge, which is the minimum flow required to inundate the high-water mark on reconstructed pre-flood topography. (B) The flood gravel on the mid-coulee butte (white circle) is crossed at a discharge of 0.9×10^6 m³ s⁻¹ on reconstructed topography. (C) Depth of the 2.2×10^6 m³ s⁻¹ discharge, which is the minimum flow required to inundate the high-water mark

on present-day (modern) topography. (D) The flood gravel on the mid-coulee butte (white circle) is crossed at a discharge of 2.2×10^6 m^3 s^{-1} on present-day topography.
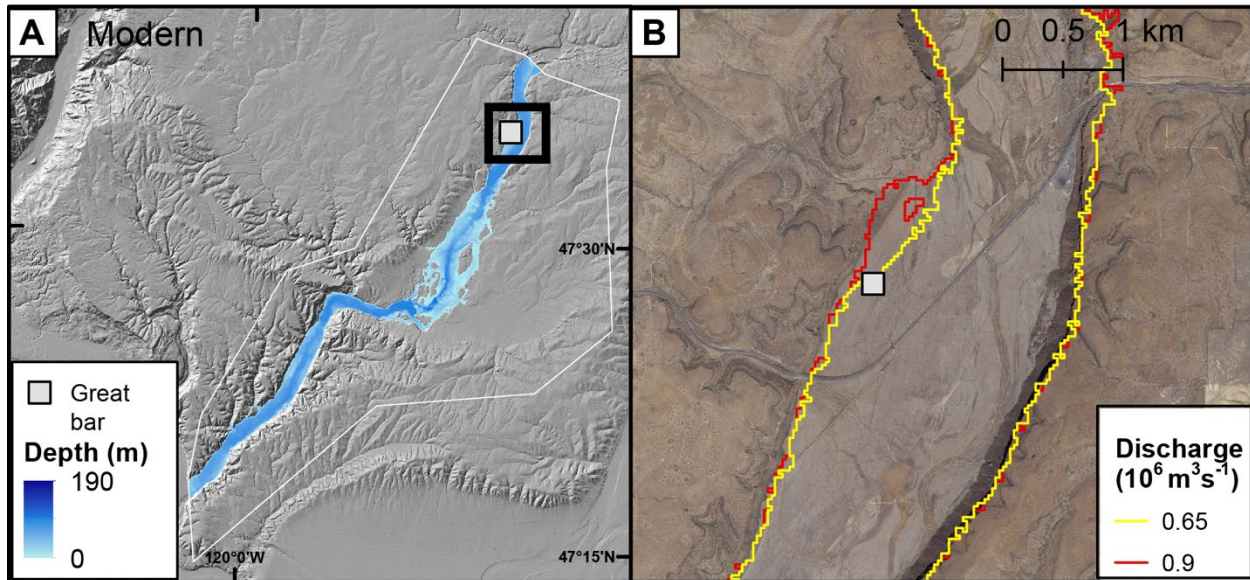
Figure S7. Discharges which come close to inundating the Great Gravel Bar in Moses Coulee. (A) Depth of the 0.9×10^6 m^3 s^{-1} discharge on the present-day (modern) topography, which is the minimum flow required to inundate the high-water mark on reconstructed pre-flood topography. (B) The top of the Great Gravel Bar (gray square) is likely inundated at a discharge close to 0.9×10^6 m^3 s^{-1} on present-day topography.
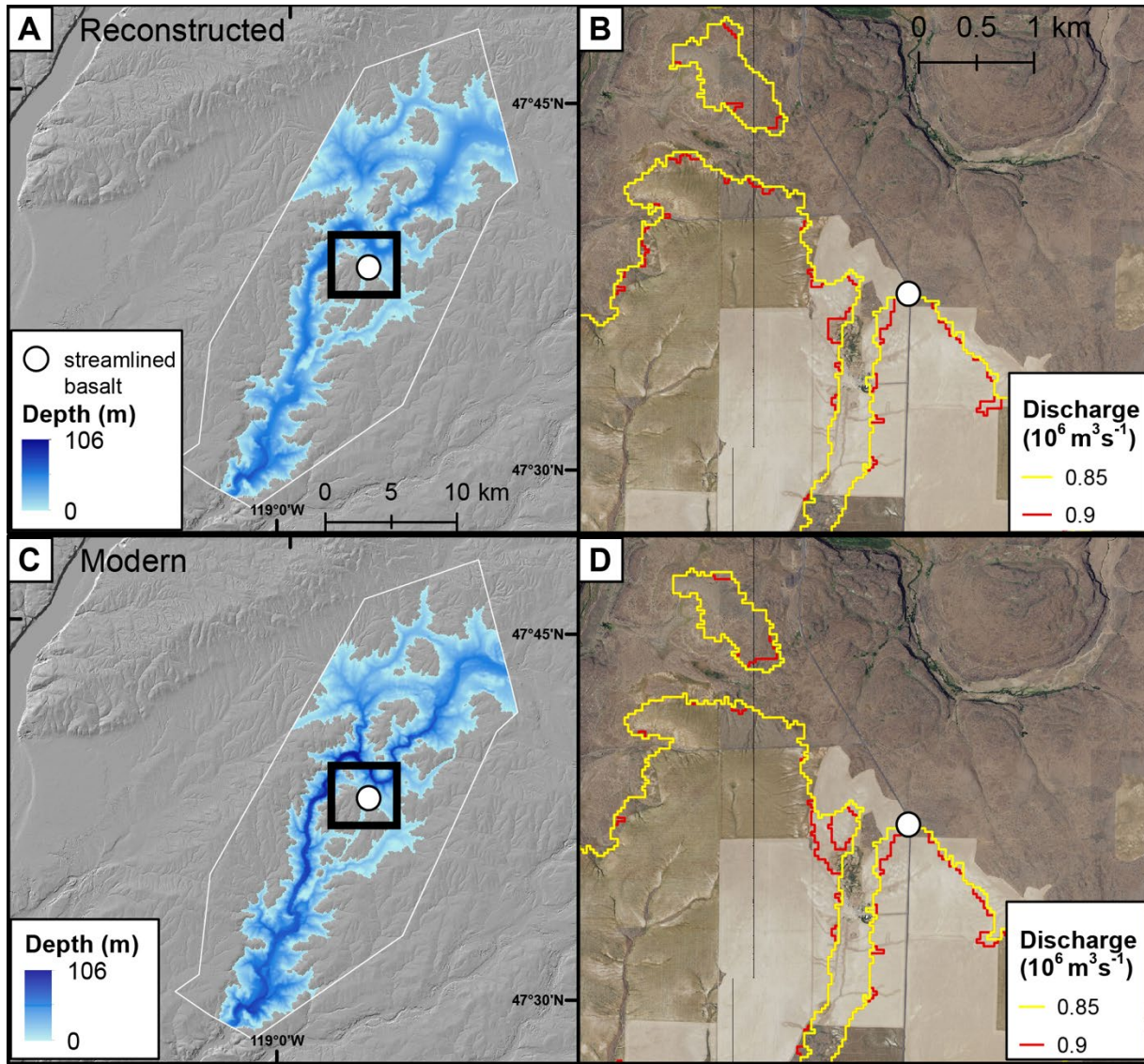
Figure S8. The high-water-inundating discharge for stripped basalt adjacent to the region of streamlined loess at Wilson Creek with lateral boundaries open. (A) Depth of the 0.9×10^6 m^3 s^{-1} discharge, which is the minimum flow required to inundate the high-water mark on reconstructed pre-flood topography. (B) The stripped (white circle) is crossed at a discharge of 0.9×10^6 m^3 s^{-1} on reconstructed topography. (C) Depth of the 0.9×10^6 m^3 s^{-1} discharge, which is the minimum flow required to inundate the high-water mark on present-day (modern) topography. (D) The stripped basalt (white circle) is crossed at a discharge of 0.9×10^6 m^3 s^{-1} on present-day topography.
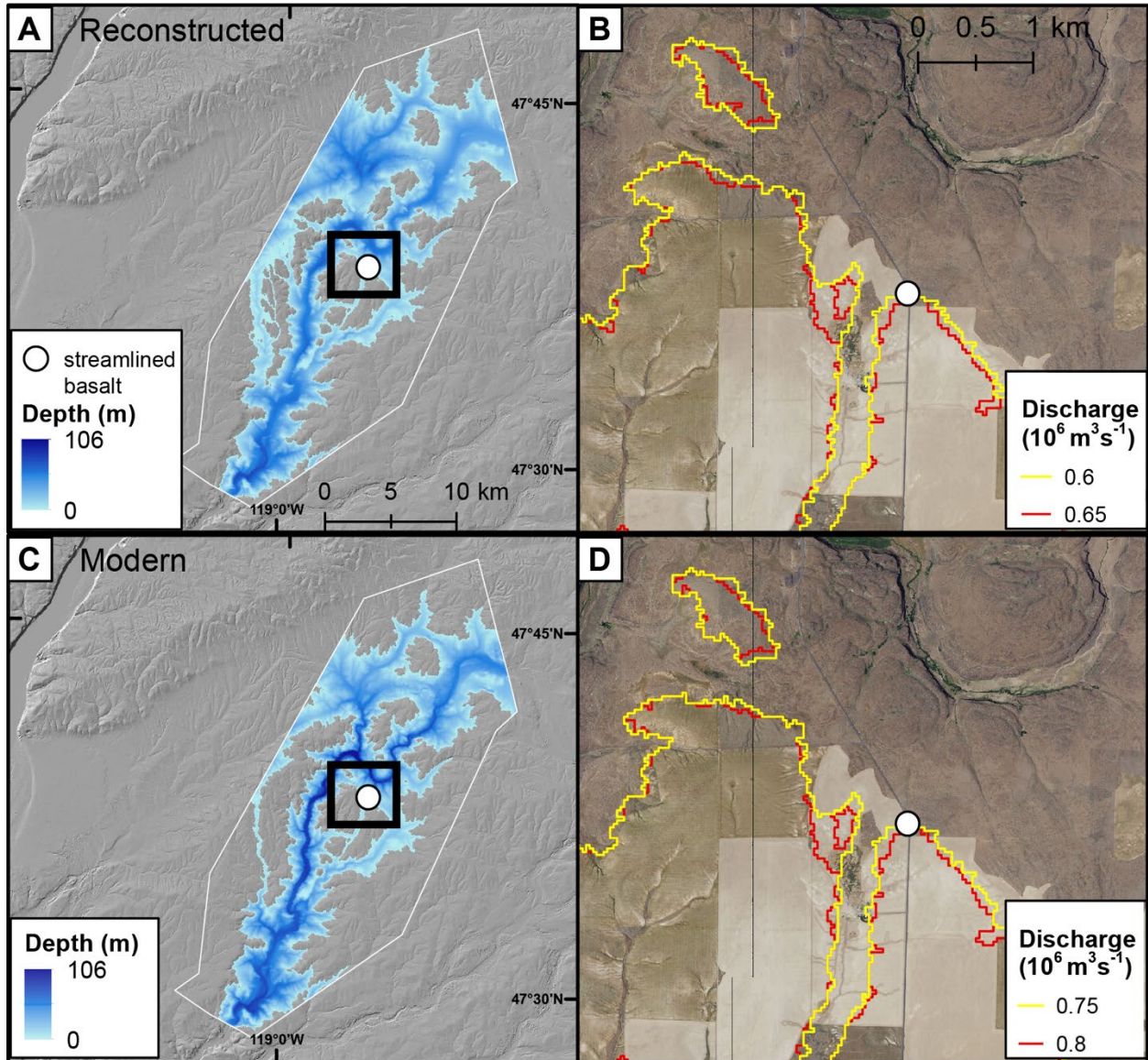
Figure S9. The high-water-inundating discharge for stripped basalt adjacent to the region of streamlined loess at Wilson Creek with lateral boundaries closed. (A) Depth of the 0.65×10^6 m^3 s^{-1} discharge, which is the minimum flow required to inundate the high-water mark on reconstructed pre-flood topography. (B) The stripped (white circle) is crossed at a discharge of 0.65×10^6 m^3 s^{-1} on reconstructed topography. (C) Depth of the 0.8×10^6 m^3 s^{-1} discharge, which is the minimum flow required to inundate the high-water mark on present-day (modern)

topography. (D) The stripped basalt (white circle) is crossed at a discharge of 0.8×10^6 m^3 s^{-1} on present-day topography.

Upper Grand Coulee

A

3.1×10^6 m^{3}s^{-1}
Discharge which
inundates crossed
drainage divide

Area averaged for flood number estimation

Shear stress (Pa)
2500

0

N

*Outlet boundary for
high-water-inundating
models*

B

0 5 10 km

0.65×10^6 m^{3}s^{-1}
Discharge which
inundates flood
gravel

C

0.9×10^6 m^{3}s^{-1}
Discharge which
inundates scarp
boulder

Moses Coulee

0 5 10 km

D

0.65×10^6 m^{3}s^{-1}
Discharge which
inundates
streamlined
basalt with
lateral boundar-
ies closed

E

0.9×10^6 m^{3}s^{-1}
Discharge which
inundates
streamlined
basalt with lateral
boundaries open

Wilson Creek

0 5 10 km
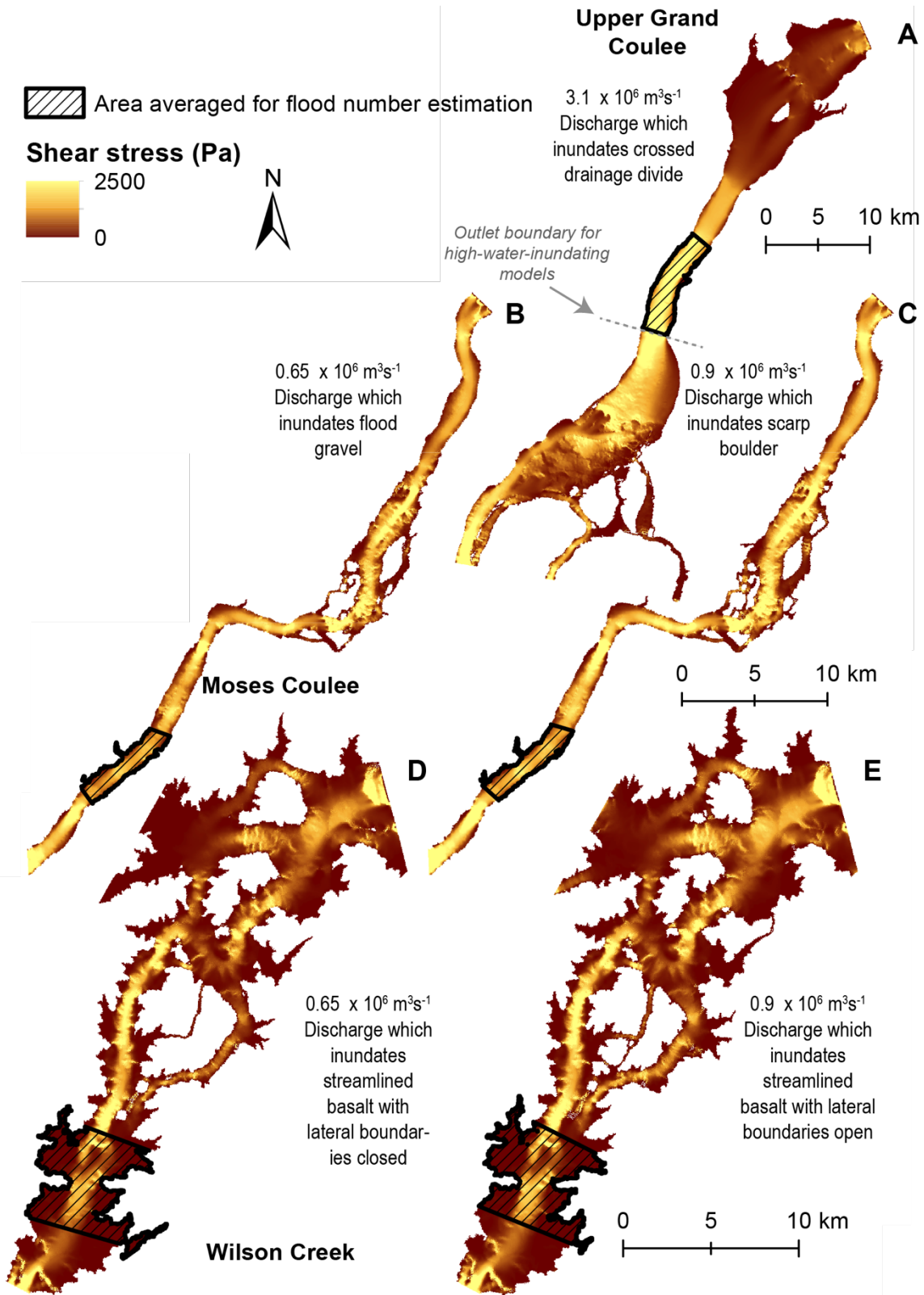
Figure S10. Shear stress maps for the high-water-inundating discharge in upper Grand Coulee (A), Moses Coulee (B & C), and Wilson Creek (D & E). The portion of the domain where shear stresses were extracted to calculate sediment fluxes are indicated by a shaded polygon. Cells with shear stress values <1 Pa or >10^5 Pa were removed, amounting to 6% of the total number of cells for upper Grand Coulee, 3-4% for Moses Coulee, and 27-35% for Wilson Creek.
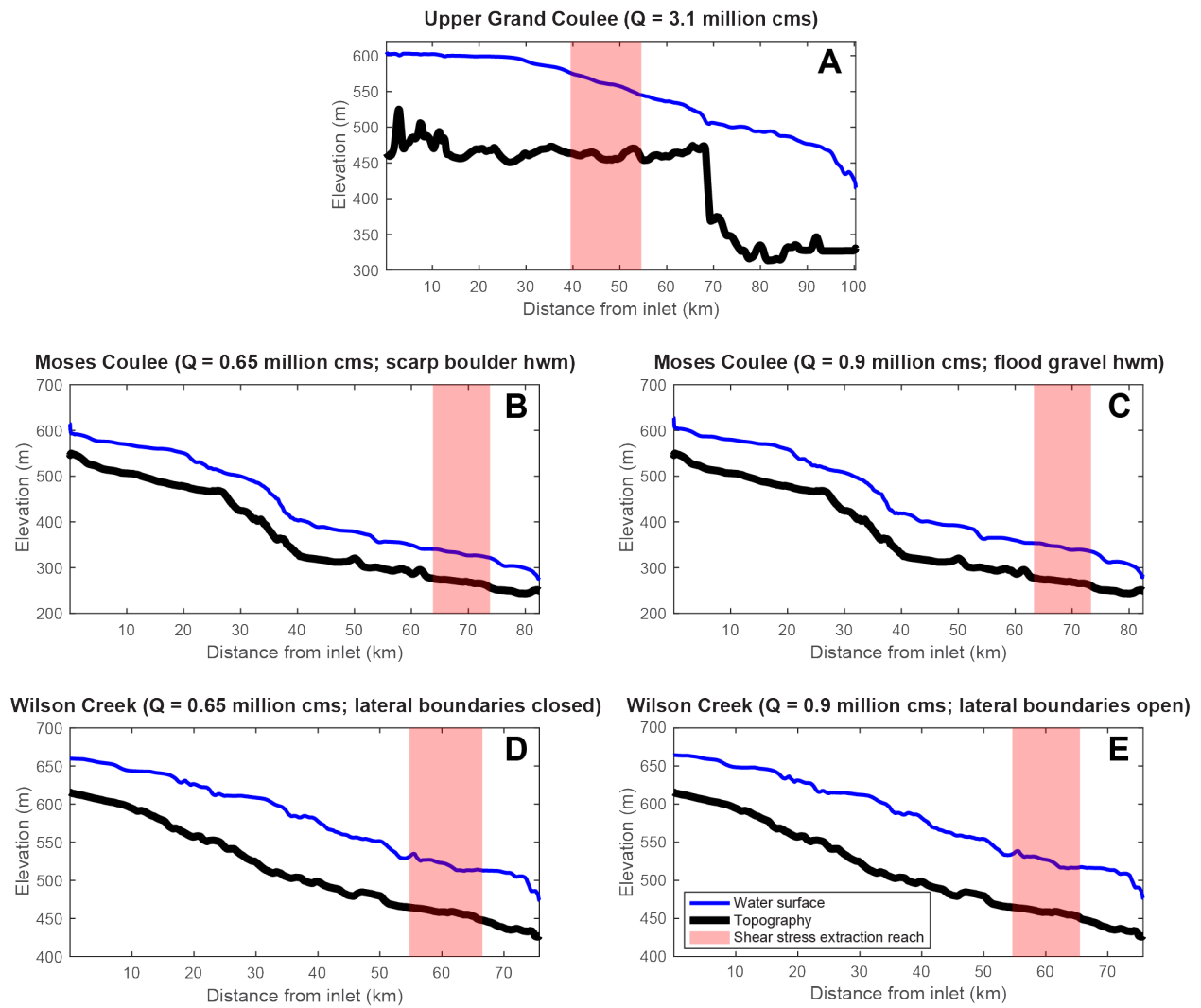
Figure S11. Long profiles along the midlines (Figure 1) of upper Grand Coulee (A), Moses Coulee (B & C), and Wilson Creek (D & E) showing stages for models of the high-water-inundating discharge from the reconstructed topography (indicated in parentheses for each

canyon) introduced onto the present-day topography. The shaded reach indicates the reach over which shear stresses were extracted in order to estimate the number of floods. Model results used to estimate the number of floods consist of non-smoothed values spanning the entire width of each canyon; however, stage and topography values extracted along the midline to produce this figure were smoothed using a 100-point moving average to reduce visual noise.
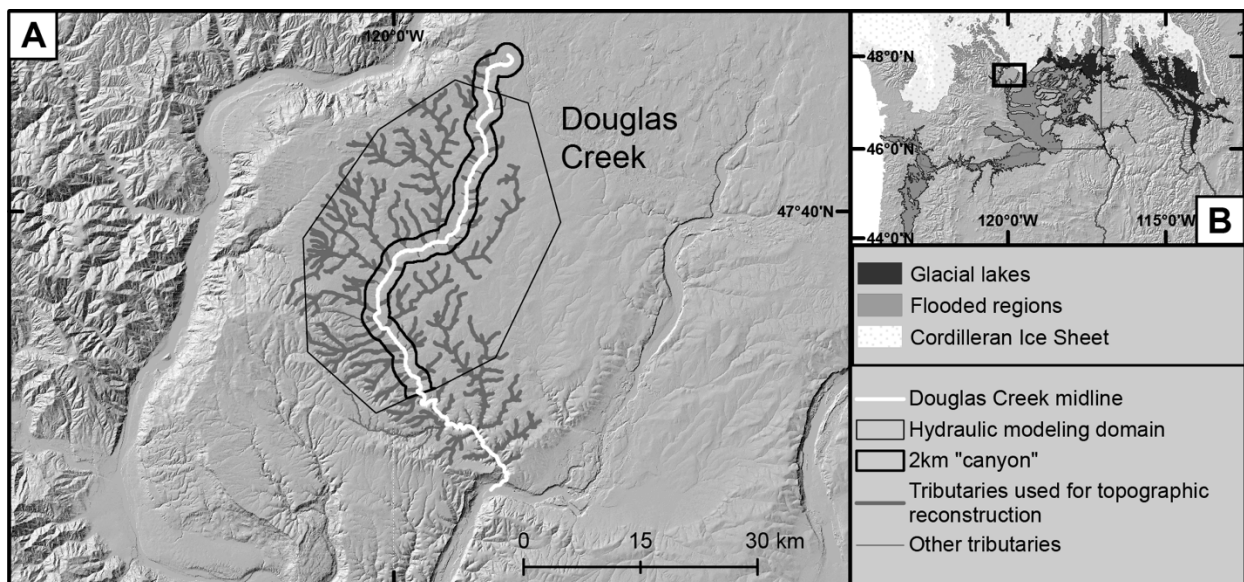
Figure S12. A) The study area showing locations of Douglas Creek where we tested our topographic reconstruction method and flood discharges. B) The location of the study area in the northwestern USA showing the locations of ice lobes, glacial lakes, and areas inundated by Missoula floods during the last glaciation (Ehlers et al., 2011).
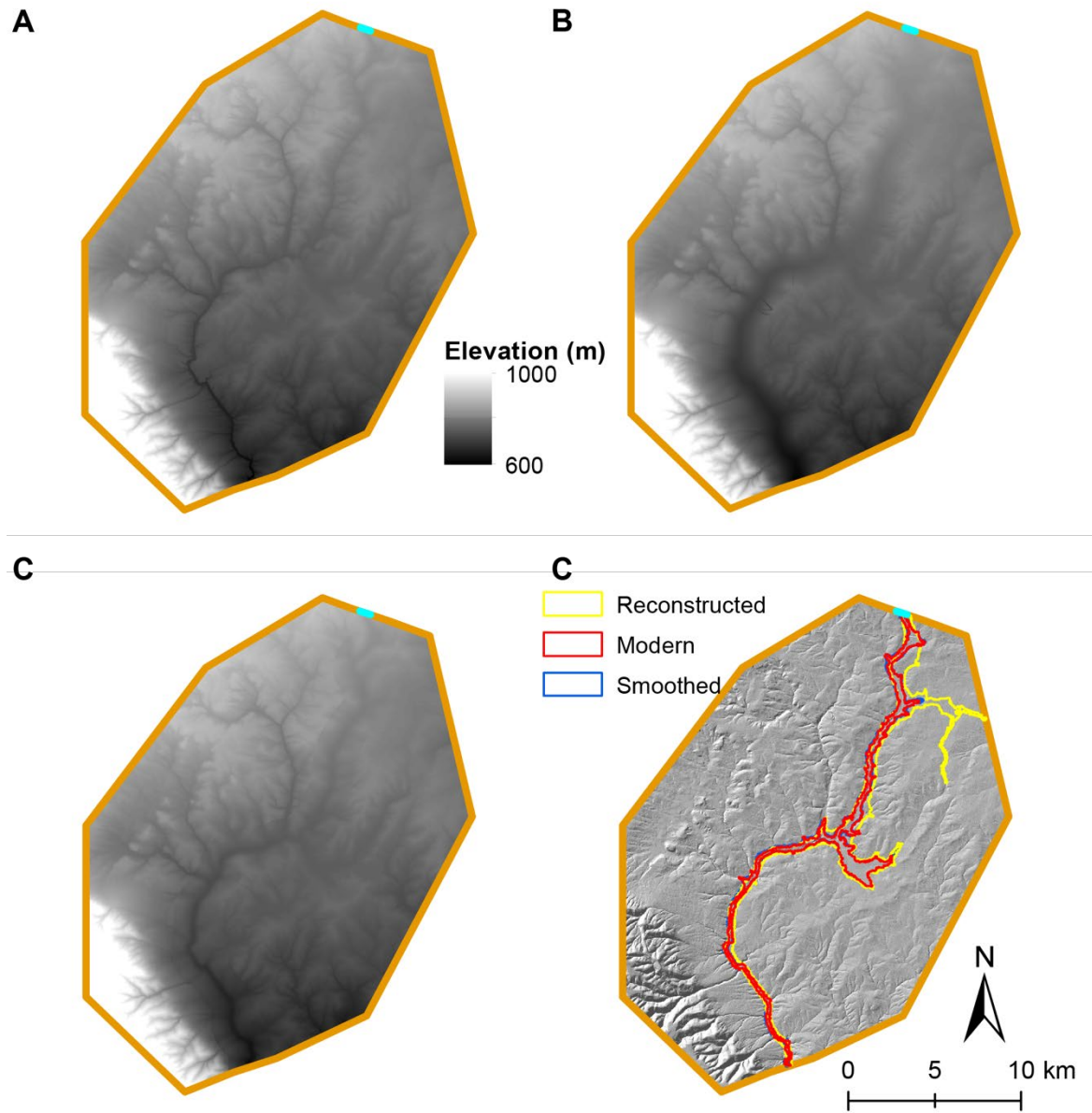
Figure S13. Boundary conditions for the present-day (modern) (A), reconstructed (B), and smoothed (C) topography of Douglas Creek, and flood inundation extents (D) using a discharge of 2,000 m^3s^{-1} on a hillshade map of the present-day topography.
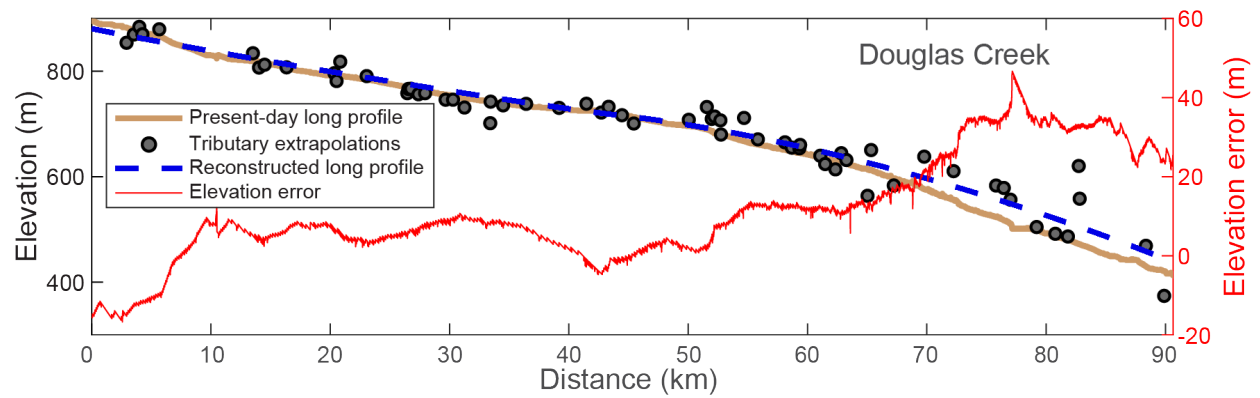
Figure S14. Reconstructed long profile for Douglas Creek showing the present-day long profile (brown line), the projected elevations of hanging tributaries (black points) which were smoothed to generate the reconstructed long profile (blue dashed line), and the elevation error (red line) between the present-day and reconstructed stream profiles.
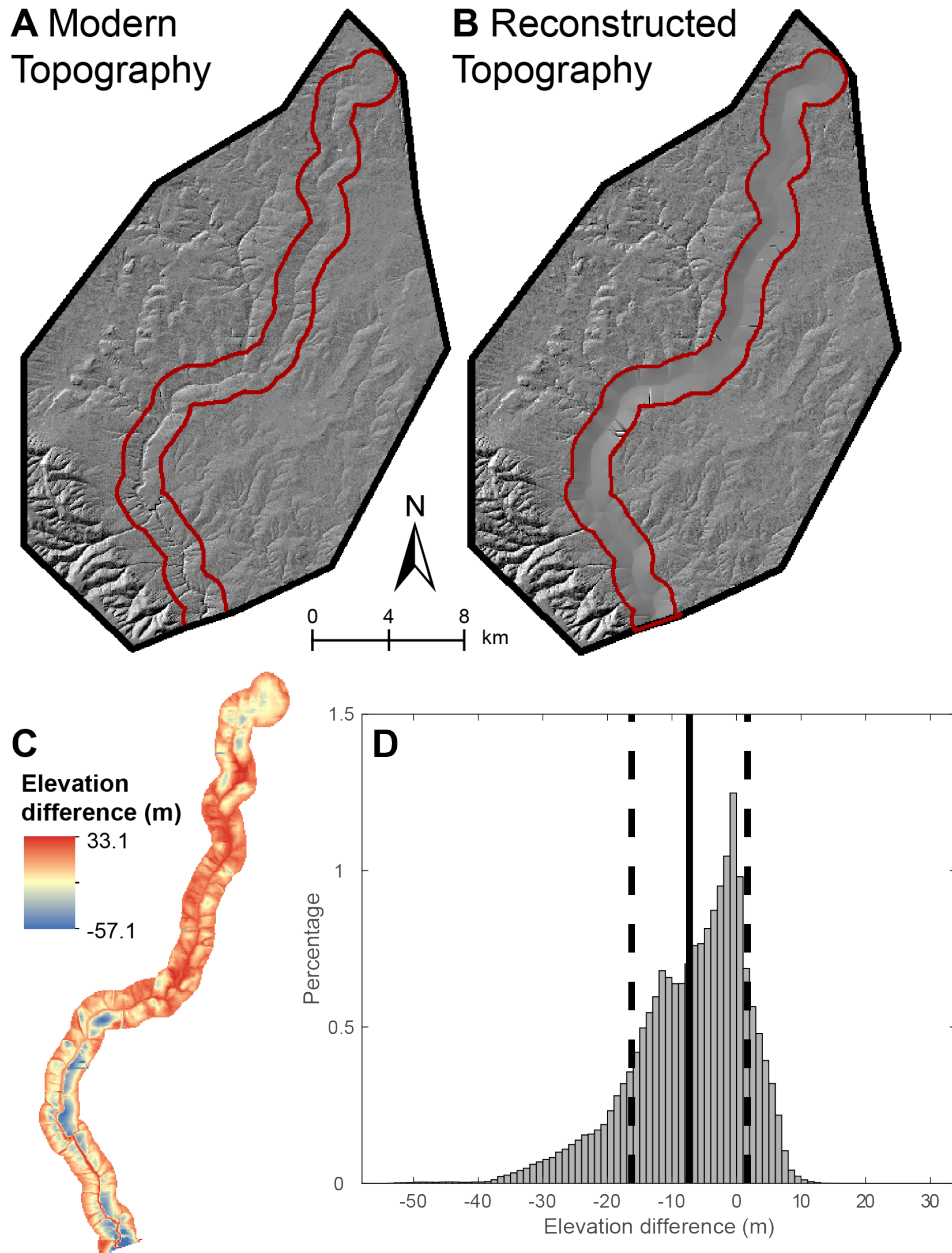
Figure S15. 2D topographic reconstruction of Douglas Creek, with present-day (modern) topography (A) and reconstructed topography (B) hillshades, with the extent of reconstruction within the 1 km buffer on either side of the stream delineated as a red polygon. The difference in elevation between the present-day and reconstructed topography is shown in C; negative (blue) values denote cells where the present-day elevation is lower than the reconstructed elevation, and positive (red) values denote cells where the present-day elevation is higher than the reconstructed

elevation. A histogram of all elevation differences in C binned into 1 m intervals is shown in D, with a thick red line at the mean value of -7.3 m, and thin red lines at ±1 standard deviation of 8.97 m from the mean.

SUPPLEMENTARY TABLES

TABLE S1. Upper Grand Coulee removed tributaries

Watershed ID	Reason for removal
2	flooded
3	glaciated
4	glaciated, short fit (3 pts)
6	flooded
7	flooded
8	glaciated
13	flooded
14	flooded
15	flooded
19	flooded
20	flooded
23	short fit (2 pts)
24	short fit (2 pts)
25	flooded
27	flooded
31	short fit (3 pts), fitted reach less than 0.5x canyon width
32	flooded
36	extrapolation distance greater than 1.5x canyon width
37	extreme λ (-2.371495)
40	extrapolation distance greater than 1.5x canyon width
49	short fit (2 pts)
50	glaciated
51	glaciated
52	glaciated
55	flooded, short fit (2 pts)
56	glaciated

Note: for tributaries removed due to "short fit," the number of binned points (either 2 or 3) is indicated in parentheses. For tributaries removed due to "extreme λ," the value of λ is indicated in parentheses.

TABLE S2. Moses Coulee removed tributaries

Watershed ID	Reason for removal
86	flooded
91	flooded
94	flooded
106	flooded
110	flooded
111	flooded
120	flooded
133	short fit (2 pts)
137	flooded, short fit (2 pts)
141	short fit (3 pts)
154	short fit (3 pts)
157	short fit (3 pts)
162	flooded
164	flooded

Note: for tributaries removed due to "short fit," the number of binned points (either 2 or 3) is indicated in parentheses. For tributaries removed due to "extreme λ," the value of λ is indicated in parentheses.

TABLE S3. Wilson Creek removed tributaries

Watershed ID	Reason for removal
231	flooded
234	flooded
235	flooded
236	flooded
238	flooded
239	flooded
240	flooded, extrapolation distance greater than 1.5x canyon width
241	extreme λ (-2.06)
242	extreme λ (-11.94)
243	flooded
247	flooded
248	flooded
249	flooded, extreme λ (0.11)
250	flooded
255	short fit (3 pts)
257	flooded
259	flooded
260	flooded
262	flooded
264	flooded
265	flooded
266	flooded
269	flooded
271	flooded
276	flooded
280	flooded
296	flooded
297	short fit (3 pts)
301	flooded
304	flooded
305	flooded
307	flooded, short fit (3 pts)
308	flooded

Note: for tributaries removed due to "short fit," the number of binned points (either 2 or 3) is indicated in parentheses. For tributaries removed due to "extreme λ," the value of λ is indicated in parentheses.

TABLE S4. SUMMARY OF ADDITIONAL MODEL RUNS

Lateral boundary conditions	High-water mark	Discharges simulated, intervals in parentheses (10^6 m^{3}s^{-1})	Number of simulated discharges	High-water-inundating discharge (10^6 m^{3}s^{-1})
upper Grand Coulee				
Open	Crossed drainage divide	Reconstructed: 0.5, 1.0-1.5 (0.05), 2.0-2.2 (0.05), 2.5-5.0 (0.25), 5.5-5.9 (0.1), 6.0-8.0 (0.5)	Reconstructed: 39	6.0
		Present-day: 1.0, 1.45, 1.9, 5-10 (1), 6.25-6.75 (0.25), 6.55-6.95 (0.05), 7.05-7.2 (0.05), 7.25-7.75 (0.25), 11-25 (1)	Present-day: 15	21
Moses Coulee				
Open	Scarp boulder & flood gravel	Reconstructed: 0.25, 0.5-1.25 (0.05), 1.5-2.5 (0.25)	Reconstructed: 22	0.65 (scarp boulder) 0.9 (flood gravel)
		Present-day: 0.25-2.0 (0.25), 0.9, 2.05-2.25 (0.05), 2.75-3.0 (0.25), 3.05-3.45 (0.05), 3.5-4.0 (0.25)	Present-day: 29	3.1 (scarp boulder) 2.2 (flood gravel)

TABLE S5. TERRESTRIAL FLOOD DEPOSITS

Thickness (ft)	Citation	Page no.	Location
300	Bretz, 1919	502	Portland delta
260	Bretz, 1928	667	Krupp (Marlin) bar
150	Bretz, 1928	674	Moses Coulee, 100 to 200 foot range
80	Bretz, 1928	674	Moses Coulee
270	Bretz, 1928	684	Arlington bar
150	Bretz, 1928	685	Jones Canyon
200	Bretz, 1928	693	Fifteen Mile Creek
290	Bretz, 1928	693	Des Chutes canyon
100	Bretz, 1928	648	Willow Creek
245	Bretz, 1928	654	Palouse Canyon
300	Bretz, 1928	651	Washtucna coulee
200	Bretz, 1928	657	Snake, two miles above mouth of Palouse River
325	Bretz, 1928	659	Snake
50	Bretz, 1928	663	Devil's Canyon
150	Bretz, 1928	664	Hardesty coulee, 100 to 200 feet of vertical range
20	Bretz, 1928	665	Reardon bar
30	Bretz, 1928	665	Reardon bar
150	Bretz, 1928	670	Upper Grand Coulee
50	Bretz, 1928	675	Babcock Bench
100	Bretz, 1928	678	Along the Columbia between Beverly and Pasco
100	Bretz, 1928	679	Northwest of Pasco
100	Bretz, 1928	680	Between Eltopia and Pasco
30	Bretz, 1928	680	Mouth of Washtucna-Esquatzel
50	Bretz, 1928	680	Between Snake and Columbia
250	Bretz, 1928	684	Arlington bar
400	Bretz, 1928	685	Jones Canyon
400	Bretz, 1928	688	John Day
300	Bretz, 1928	693	Rufus
35	Bretz, 1928	694	Along road from Fairbanks station, 30-40 feet range
100	Bretz, 1928	695	Petersburg bar
250	Bretz, 1928	695	Mosier bar
50	Bretz, 1929	398	Kamiache Creek
75	Bretz, 1929	401	Palouse Canyon
15	Bretz, 1929	401	Lancaster Creek
80	Bretz, 1929	408	Central Ferry
60	Bretz, 1929	410	Central Ferry
75	Bretz, 1929	421	Lewiston residential section, 50-100 feet range
200	Bretz, 1930	398	Trinidad
200	Bretz, 1930	403	Willow Springs
175	Bretz, 1930	406	Vantage bridge

175	Bretz, 1930	418	Corral Canyon
40	Bretz, 1930	419	Chandler Narrows
128	Bretz et al., 1956	969	Quincy Basin, max.
60	Bretz et al., 1956	983	Crab Creek, Quincy basin, 50-70 feet range
5	Bretz et al., 1956	999	Evergreen Summit
150	Bretz et al., 1956	1000	Staircase Rapid
100	Bretz et al., 1956	1014	Priest Rapids bar, 75-125 feet range
100	Bretz et al., 1956	968	Bacon syncline
109	Bretz et al., 1956	969	Soap Lake drilling
120	Bretz et al., 1956	978	Bar no. 1, upper Crab Creek, bar summit relative to valley floor
70	Bretz et al., 1956	978	Bar no. 2, upper Crab Creek, 60-80 feet above valley floor
94	Bretz et al., 1956	978	Bar no. 3, upper Crab Creek, bar summit relative to valley floor
70	Bretz et al., 1956	979	Bar no. 4, upper Crab Creek, 40-100 feet above valley floor
150	Bretz et al., 1956	980	Wilson Creek, only elevation of highest bar reported
60	Bretz et al., 1956	982	Black Rock Coulee, at least 50-70 feet thick
88	Bretz et al., 1956	983	Lind Coulee
112.5	Bretz et al., 1956	993	Beverly Bar, 100 to 125 feet above sump and Columbia River
28	Bretz et al., 1956	996	Bar on Taunton-Anson terrace
10	Bretz et al., 1956	998	Flat 2 miles west of Mesa
40	Bretz et al., 1956	1003	Washtucna Coulee
40	Bretz et al., 1956	1004	Just west of Sulphur Lake, elevation of bar top 50 feet above valley bottom and 30 feet above closed depression
180	Bretz et al., 1956	1005	Fill at Connell
50	Bretz et al., 1956	1007	South of Mesa

TABLE S6. MEDIAN NUMBER OF FLOODS PREDICTED WITH OTHER SEDIMENT RATIOS

Canyon	$q_s/q_b = 8.3$	$q_s/q_b = 4.56$	$q_s/q_b = 2.36$
Upper Grand Coulee	6	10	16
Moses Coulee	6	11	17
Wilson Creek	13	21	35

Note: q_s/q_b of 8.3 is the ratio of offshore fine-grained flood deposit volume to the volume of coarse-grained terrestrial flood deposits, q_s/q_b of 4.56 is the largest ratio of suspended to bedload sediment reported in Turowski et al. (2010) from modern outburst floods from catchments dammed by landslides or glaciers, and q_s/q_b of 2.36 is the average ratio of suspended to bedload sediment reported in Turowski et al. (2010) from modern outburst floods from catchments dammed by landslides or glaciers. All flood numbers are rounded up to the nearest whole number.

	median shear stress (Pa)[*]	bedload flux (m^3s^{-1})		suspended sediment flux (m^3s^{-1})		total sediment flux (m^3s^{-1})		average canyon width (m)	volumetric flux (m^3s^{-1})		duration (s)		number of floods	
		upper bound	lower bound	upper bound	lower bound	upper bound	lower bound		upper bound	lower bound	upper bound	lower bound	upper bound	lower bound
upper Grand Coulee														
	2276±5	1.03 (1.09)	1.02 (1.09)	8.52 (9.09)	8.46 (9.02)	9.54 (10.2)	9.47 (10.1)	3460	33021 (35229)	32783 (34986)	2.05E+06 (1.92E+06)	2.07E+06 (1.94E+06)	6 (6)	6 (6)
Moses Coulee														
scarp boulder	1049±5	0.29 (0.34)	0.29 (0.33)	2.42 (2.80)	2.38 (2.76)	2.71 (3.14)	2.67 (3.09)	2005	5442 (6296)	5352 (6201)	2.67E+06 (2.31E+06)	2.71E+06 (2.34E+06)	8 (7)	8 (7)
flood gravel	1180±6	0.36 (0.40)	0.35 (0.40)	2.95 (3.36)	2.90 (3.31)	3.31 (3.76)	3.25 (3.70)	2171	7180 (8164)	7065 (8044)	2.04E+06 (1.78E+06)	2.06E+07 (1.80E+06)	6 (5)	6 (5)
Wilson Creek[†]														
lateral boundaries closed	157±7	0.00 (0.02)	0.00 (0.01)	0.03 (0.14)	0.01 (0.12)	0.03 (0.16)	0.02 (0.14)	4987	140 (782)	83 (674)	1.12E+07 (2.00E+06)	1.90E+07 (2.32E+06)	31 (6)	53 (7)
lateral boundaries open	174±6	0.00 (0.02)	0.00 (0.02)	0.04 (0.17)	0.03 (0.15)	0.05 (0.19)	0.03 (0.16)	5295	238 (981)	168 (864)	6.57E+06 (1.60E+06)	9.34E+06 (1.81E+06)	19 (5)	26 (5)

Note: Calculations use a grain size D_{50} = 0.15 m measured on the surface of the boulder bar on Moses Coulee (Larsen and Lamb, 2016). Values which use a grain size D_{50} = 0.03 m, from the D_{50} measured on the surface of the boulder bar on Moses Coulee (Larsen and Lamb, 2016) divided by an armoring ratio of 4.8 (King, 2004, p. 200), are included in parentheses if different from those which use the larger D_{50} of 0.15 m. All flood numbers are rounded up to the nearest whole number of floods.

[*]Median shear stress and standard error are calculated for cells with depths >0.5 m in a 10 km reach of each canyon (Figure S11).

[†]The distribution of flood numbers for Wilson Creek yields a median of 13 floods and a 95th percentile of 14 floods. The lower bound of the range of floods was adjusted to be one flood, as a single flood is the smallest number of physically possible floods. Estimates of erosion rate and waterfall retreat rate referenced in the main text are based off this adjusted range of 1 – 27 floods rather than the -1 – 27 floods implied by the range of 13±14 floods generated from the median and 95th percentile values of estimated flood numbers.

TABLE S8. SENSITIVITY OF BIN WIDTH AND SMOOTHING DISTANCE

| Tributary ID | Elevations (m) extrapolated 500 m from the canyon rim | | | | | Rim elevations (m) | | | | |
| | Bin width (m) | | | | | Smoothing window | | | | |
	25 m fixed	50 m fixed	100 m fixed	200 m fixed	$10^{bin\ number}$	5 m	10 m	25 m	50 m	no smoothing
4	645	646	645	583	664	719	719	719	719	719
27	596	596	596	601	595	690	690	690	690	690
29	608	607	608	609	616	723	723	723	723	723
38	563	562	562	562	562	730	730	730	730	730
51	700	696	699	705	657	783	783	783	783	783
53	673	673	673	673	671	731	731	731	731	731
122	420	416	412	423	481	675	675	675	675	675
123	433	434	434	431	416	614	614	614	614	614
180	563	568	565	567	478	761	761	761	761	761
256	514	514	514	516	508	624	624	624	624	624
257	490	490	491	505	480	604	604	604	604	604

Note: For bin width, the elevation given is the elevation extrapolated 500 m from the rim point. For smoothing window, the elevation given is the elevation at the rim point.

SUPPLEMENTARY REFERENCES

Bretz, J.H., 1928, Bars of Channeled Scabland: Geological Society of America Bulletin, v. 39, p. 643–701.

Bretz, J.H., 1919, The late Pleistocene submergence in the Columbia Valley of Oregon and Washington: The Journal of Geology, v. 27, p. 489–506.

Bretz, J.H., 1929, Valley deposits immediately east of the Channeled Scabland of Washington: Journal of Geology, v. 37, p. 393–541.

Bretz, J.H., 1930, Valley deposits immediately west of the Channeled Scabland: Journal of Geology, v. 38, p. 385–422.

Bretz, J.H., Smith, H.T.U., and Neff, G.E., 1956, Channeled Scabland of Washington: new data and interpretations: Geological Society of America Bulletin, v. 67, p. 957–1049.

Ehlers, J., Gibbard, P.L., and Hughes, P.D., 2011, Quaternary Glaciations - Extent and Chronology: Elsevier, v. 15, 1126 p.

Hanson, L.G., 1970, The Origin and Development of Moses Coulee and Other Scabland Features on the Waterville Plateau [PhD Thesis]: 140 p.

Hutchinson, M.F., Xu, T., and Stein, J.A., 2011, Recent progress in the ANUDEM elevation gridding procedure, *in* Hengel, T., Evans, I.S., Wilson, J.P., and Gould, M. eds., Redlands, CA, Geomorphometry, p. 19–22.

King, J.G., 2004, Sediment transport data and related information for selected coarse-bed streams and rivers in Idaho: Department of Agriculture, Forest Service General Technical Report RMRS-GTR-131, 26 p.

Larsen, I.J., and Lamb, M.P., 2016, Progressive incision of the Channeled Scablands by outburst floods: Nature, v. 538, p. 229–232.

Lehnigk, K.E., and Larsen, I.J., 2022, Pleistocene megaflood discharge in Grand Coulee, Channeled Scabland, USA: Journal of Geophysical Research: Earth Surface, v. 127.

Savitzky, A., and Golay, M.J.E., 1964, Smoothing and differentiation of data by simplified least squares procedures: Analytical Chemistry, v. 36, p. 1627–1639.

Turowski, J.M., Rickenmann, D., and Dadson, S.J., 2010, The partitioning of the total sediment load of a river into suspended load and bedload: A review of empirical data: Sedimentology, v. 57, p. 1126–1146.

Washington State Department of Natural Resources, 2010, Digital Geology of Washington State at 1:100,000 Scale version 3.0: Division of Geology and Earth Resources GIS data.